

X-ray structure of a vanadium-containing enzyme: Chloroperoxidase from the fungus *Curvularia inaequalis*

(halogenation/bromoperoxidase/crystallography/coordination chemistry)

ALBRECHT MESSERSCHMIDT* AND RON WEVER†

*Max Planck Institute of Biochemistry, D-82152 Martinsried, Germany; and †E. C. Slater Institute, Department of Biochemistry, University of Amsterdam, 1018 TV Amsterdam, The Netherlands

Communicated by Robert Huber, Max-Planck-Institut für Biochemie, Martinsried, Germany, August 7, 1995 (received for review June 3, 1995)

ABSTRACT The chloroperoxidase (EC 1.11.1.-) from the fungus *Curvularia inaequalis* belongs to a class of vanadium enzymes that oxidize halides in the presence of hydrogen peroxide to the corresponding hypohalous acids. The 2.1 Å crystal structure ($R = 20\%$) of an azide chloroperoxidase complex reveals the geometry of the catalytic vanadium center. Azide coordinates directly to the metal center, resulting in a structure with azide, three nonprotein oxygens, and a histidine as ligands. In the native state vanadium will be bound as hydrogen vanadate(V) in a trigonal bipyramidal coordination with the metal coordinated to three oxygens in the equatorial plane, to the OH group at one apical position, and to the $\epsilon 2$ nitrogen of a histidine at the other apical position. The protein fold is mainly α -helical with two four-helix bundles as main structural motifs and an overall structure different from other structures. The helices pack together to a compact molecule, which explains the high stability of the protein. An amino acid sequence comparison with vanadium-containing bromoperoxidase from the seaweed *Ascophyllum nodosum* shows high similarities in the regions of the metal binding site, with all hydrogen vanadate(V) interacting residues conserved except for lysine-353, which is an asparagine.

Haloperoxidases form a class of enzymes that are able to oxidize halides (Cl^- , Br^- , I^-) in the presence of hydrogen peroxide to the corresponding hypohalous acids according to



If a convenient nucleophilic acceptor is present, a reaction will occur with HOX to form a diversity of halogenated reaction products. Many of these organohalogenes have biocidal effects and thus may provide defense functions.

As has only been recently discovered (1, 2), some of the haloperoxidases contain vanadium in the active site. These enzymes are widespread in the marine environment and have been found in a variety of seaweeds (3).

Recently, it was shown (4) that the chloroperoxidase (CPO) secreted by the fungus *Curvularia inaequalis* is also a vanadium enzyme with properties similar to the bromoperoxidase. This CPO forms HOCl as a product (5), which is a strongly bactericidal and oxidizing agent. The fungus belongs to the group of dematiaceous hyphomycetes, which are pathogenic toward plants and/or are saprophytes, and it has been suggested (6) that the enzyme and its product are used in a mechanism to oxidize plant cell walls to facilitate penetration of the fungus into the host.

The vanadium bromoperoxidases have been studied in great detail using a variety of biophysical techniques (7) including extended x-ray absorption fine structure (8, 9) and electron spin echo envelope modulation (10, 11). Vanadium(IV) or

Table 1. Data collection and phasing statistics

Parameter	Native	APWO	APHG
Diffraction data			
Resolution	2.1 Å	2.3 Å	2.3 Å
Total observations	132,089	103,740	101,456
Unique reflections	42,197	32,289	31,231
Completeness (%)*	98.9/96.8	99.6/98.2	96.4/66.3
R_{merge}^\dagger	0.094	0.084	0.078
R_{F}^\ddagger	0.056	0.069	0.052
MIRAS phasing			
Number of sites		1	1
R_{iso} (20 to 3.0 Å) §		0.110	0.078
R_{Cullis} acentric (20 to 3.5 Å) $^\parallel$		0.66	0.80
Phasing power acentric (20 to 3.5 Å) $^\parallel$		1.80	1.40
FOM acentric (20 to 3.5 Å) **	0.565		

The abbreviations represent the following treatments: APWO, apoenzyme was produced by dialysis of protein (1.6 mg/ml) in 50 mM Tris-HCl (pH 8.3) against a solution containing 0.1 M citrate, 0.1 M phosphate, and 10 mM EDTA (pH 3.8) followed by a dialysis against a 50 mM Tris-H₂SO₄ (pH 8.3) buffer solution. Before crystallization, Na₂WO₄ was added to the start protein solution (8 mg/ml) at 2 mM. Further crystallization conditions were identical to the native protein. APHG, native CPO crystals were soaked in normal mother liquor plus 2 mM 1,10-phenanthroline for 1 day to remove possible Zn contamination. Then the crystals were soaked in mother liquor plus 2 mM mercury acetate. MIRAS, multiple isomorphous replacement anomalous scattering.

*20–2.1/2.14–2.10 Å and for derivatives 20–2.3/2.38–2.3 Å.

$^\dagger R_{\text{merge}} = \sum \sum |I(h)_i - \langle I(h) \rangle| / \sum \sum I(h)_i$, where $I(h)_i$ is the observed intensity in the i th source and $\langle I(h) \rangle$ is the mean intensity of reflection h over all measurements of $I(h)$.

$^\ddagger R_{\text{F}} = R_{\text{merge}}$ after independent averaging of Friedel pairs.

$^\S R_{\text{iso}} = \sum |F_{\text{PH}} - F_{\text{P}}| / \sum F_{\text{P}}$, where F_{P} and F_{PH} are the scaled structure factor amplitudes of a reflection from the native and heavy atom derivative, respectively.

$^\parallel R_{\text{Cullis}} = \sum |F_{\text{PH}} \pm F_{\text{P}}| - F_{\text{H}} / \sum |F_{\text{PH}} - F_{\text{P}}|$, where F_{H} is the calculated heavy atom structure factor amplitude.

$^\parallel$ Phasing power = $\langle F_{\text{H}} \rangle / \langle E \rangle$, where $\langle F_{\text{H}} \rangle$ is the rms of the heavy atom structure factor and $\langle E \rangle$ is the rms lack of closure summed over the reflections used in the heavy atom refinement.

** Figure of merit prior to density modification.

(III) states have not been observed by EPR or K-edge x-ray studies in the presence of substrates or during turnover, and the reduced enzyme is inactive. Apparently the redox state of the metal does not change during catalytic turnover, and a model has been suggested (11) in which the vanadium site functions by binding hydrogen peroxide to yield an activated peroxy intermediate, which is able to react with bromide to produce HOBr. Similar models have now been proposed (12, 13) for a number of metal-catalyzed oxidations of bromide by hydrogen peroxide.

A detailed kinetic study of the formation of HOCl by the chloroperoxidase (5) revealed many similarities with the ki-

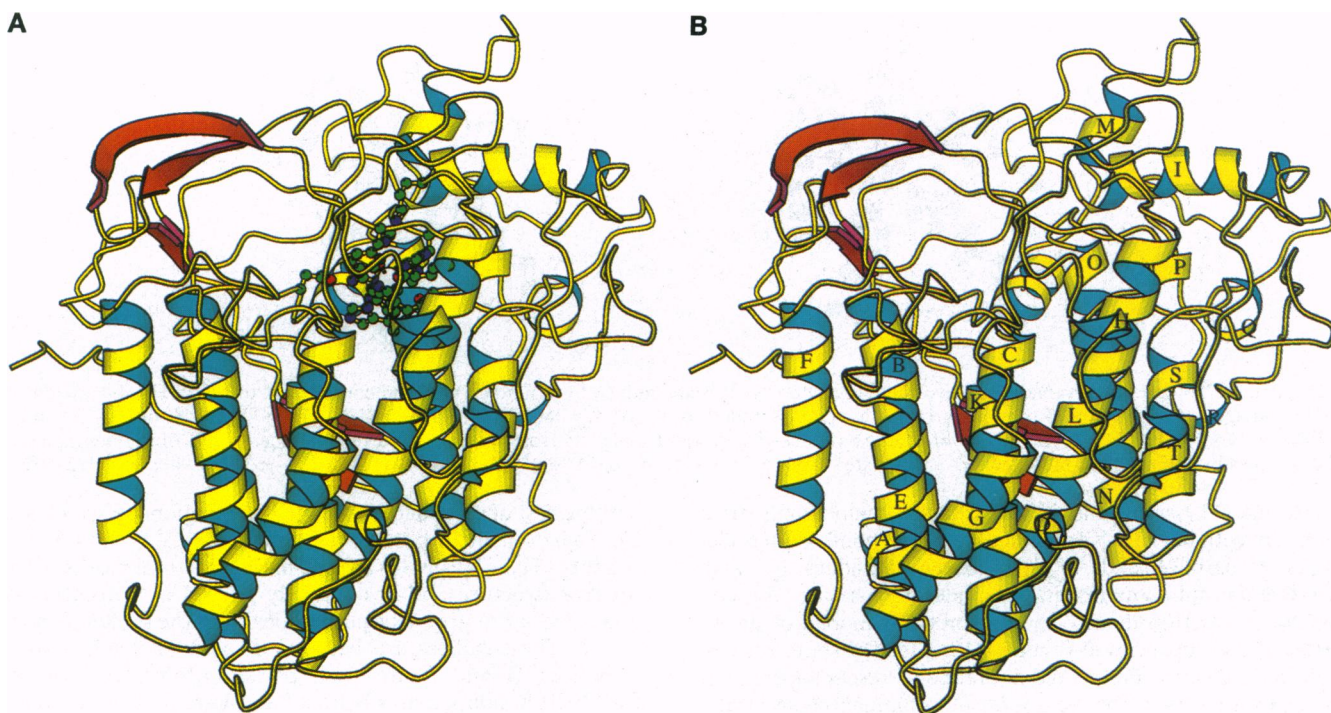


FIG. 1. Ribbon-type representation of the CPO molecule [MOLSCRIPT (26)]. (A) Molecule plus vanadium binding site. (B) Molecule without metal site and with labeling of helices.

netics of the vanadium bromoperoxidase. Azide was found to be a weak inhibitor for the vanadium-containing marine bromoperoxidase (14).

MATERIALS AND METHODS

The CPO from *C. inaequalis*. The isolation, purification, and biochemical characterization of the CPO from the fungus *C.*

inaequalis have been reported (4, 5, 15). The amino acid sequence has recently been determined by cDNA sequencing techniques (6), and the mature enzyme consists of 609 amino acid residues with a calculated molecular mass of 67,488 Da.

Crystallization, Data Collection, and Structure Determination. Hanging droplets were made from 7.5 μ l of a protein solution (8.7 mg/ml) in 5 mM Mops (pH 8.1) and 1 mM Na_3VO_4 and 2.5 μ l of precipitating buffer containing 1.5 M $(\text{NH}_4)_2\text{SO}_4$ in 0.1 M Tris-HCl plus 0.02% NaN_3 (pH 8.0). Crystallization was achieved at 21°C by vapor diffusion against 1.6 M $(\text{NH}_4)_2\text{SO}_4$ in 0.1 M Tris-HCl plus 0.02% NaN_3 (pH 8.0). Rhombohedral-shaped crystals of ≈ 0.3 mm appeared after 3 days. They were harvested in 2.0 M $(\text{NH}_4)_2\text{SO}_4/0.1$ M Tris-HCl/0.02% NaN_3 (pH 8.0) for data collection of the native form (see Table 1). The crystals diffracted to 2.1 Å resolution and belonged to the space group R3 with lattice constants $a = b = 131.69$ Å, $c = 112.97$ Å, $\alpha = \beta = 90^\circ$, $\gamma = 120^\circ$. All x-ray measurements were done on a Hendrix/Lentfer x-ray image-plate system (Mar-Research, Hamburg, Germany) mounted on a Rigaku rotating anode generator operated at 5.4 kW ($\lambda = \text{CuK}\alpha = 1.5418$ Å) and at 16°C. The x-ray intensities were processed with MOSFLM (16) and programs from the CCP4 suite (17). Heavy atom derivatives were prepared as described in Table 1 and were analyzed by difference Patterson methods and cross-phased difference Fourier maps with PROTEIN (18). Heavy atom sites and phases were refined with MLPHARE (19). Phases were improved and extended from 3.5 Å to 2.5 Å resolution by the density modification routines of the CCP4 suite (17). Skeletonized electron density maps (20) were used to identify the molecular envelope and to locate secondary structure. The program o (21) was used on an ESV-30 Graphic system workstation (Evans & Sutherland, Salt Lake City) for all model building. The model was refined by energy-restrained crystallographic refinement with XPLOR (22), and the parameters were derived by Engh and Huber (23). Equilibrium bond distances and bond angles for the vanadium site were taken from hydrogen vanadate (24) and from a vanadium(V) complex containing bound azide (25). Weak restraints (1/10th of corresponding parameters) were applied to the metal site. The current model has been refined to a crystallographic R factor of 20.0% with all data from 8.0 to 2.1 Å resolution (41,486 unique reflections) and comprises 4485 nonhydrogen protein atoms, 429 water oxygen

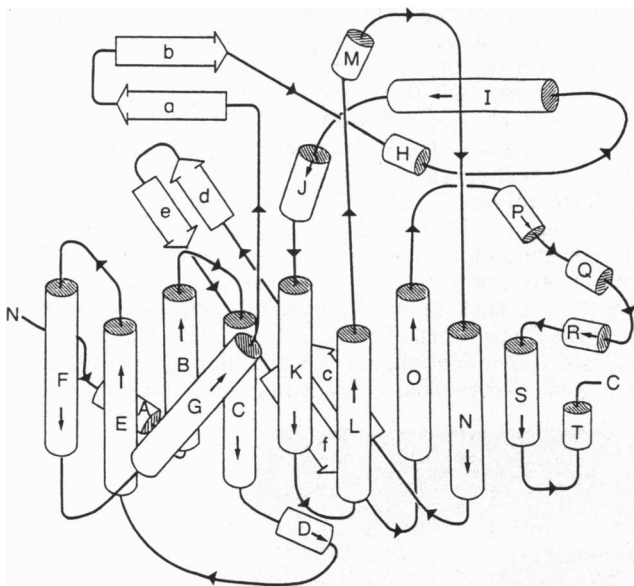


FIG. 2. Schematic drawing of the secondary structure elements of CPO. All helices are drawn as cylinders; β -strands are depicted as arrows. Amino acids in secondary structure elements are 3_{10}A , 16–20; αB , 22–40; αC , 47–68; 3_{10}D , 85–87; αE , 98–114; αF , 131–147; αG , 157–173; βa , 202–207; βb , 210–218; αH , 226–229; αI , 254–268; αJ , 280–288; αK , 300–314; αL , 325–356; αM , 361–366; αN , 403–419; βc , 436–440; βd , 449–451; βe , 466–468; βf , 473–476; αO , 479–492; αP , 498–501; αQ , 504–507; 3_{10}R , 530–532; αS , 552–565; 3_{10}T , 572–576. The N and C termini are indicated.

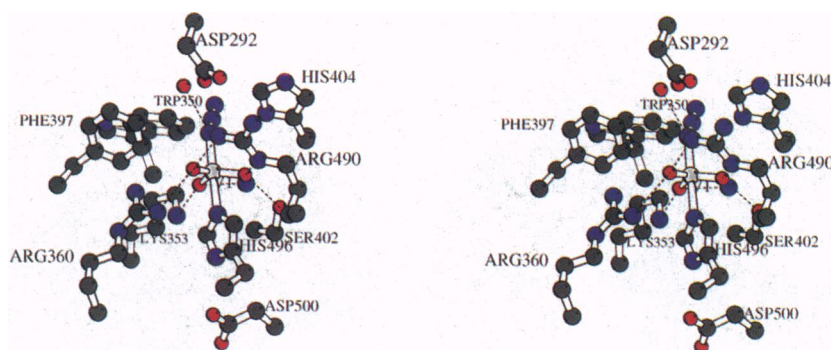


FIG. 3. Stereoview of the vanadium active site [MOLSCRIPT (26)]. Vanadium(V) is bound as VO_3 and coordinated to $\text{N}^{\delta 2}$ of His-496 and N^1 of the bound azide. Oxygen $\text{O}^{\omega 1}$ of the VO_3 group is hydrogen bonded to $\text{N}^{\eta 1}$ of Arg-360 and $\text{N}^{\eta 2}$ of Arg-490, oxygen $\text{O}^{\omega 2}$ to N^{ζ} of Lys-353 and N of Gly-403, and oxygen $\text{O}^{\omega 3}$ to O^{γ} of Ser-402 and N^{ϵ} of Arg-490. A water molecule from solvent is hydrogen bonded to N^1 of the bound azide. The residues building up the metal center are donated from helices J, L, N, and O and from turns 290–294, 355–363, 395–406, and 492–502.

atoms, one VO_3 group, and one azide ion maintaining strict geometry with deviations from ideal values of bond lengths and angles of 0.012 \AA and 1.7° , respectively. Residues 1–2 and 579–609 are not contained in the model because they are not defined by electron density and are probably mobile or disordered. The occupancies of residues 118–127 were set to zero as their initial electron density did not refine to a clear appearance for this external loop. The average B factors for main chain atoms, side chain atoms, and solvent molecules are 20.4, 22.1, and 40.3 \AA^2 , respectively.[‡]

An x-ray data set of a crystal grown with azide-free buffer was collected to a resolution of 2.0 \AA on the same experimental setup and processed as described before. Model coordinates omitting the VO_3 and azide groups were refined against the F_o values of the azide-free form, and a corresponding $|F_o| - |F_c|$ difference Fourier map was calculated.

RESULTS AND DISCUSSION

Overall Protein Structure. The structure solved by multiple isomorphous replacement techniques (Table 1) reveals one molecule per asymmetric unit. The molecule has an overall cylindrical shape with a length of about 80 \AA and a diameter of 55 \AA (Fig. 1A). The molecules are arranged in the crystals as trimers around the crystallographic threefold axis. The secondary structure, which was analyzed with the program DSSP (27), is mainly helical (about 44% of the atomic model), consisting of 20 helices, a small part of β -structures (six short β -strands, pairwise arranged as three antiparallel β -ladders),

and the rest of extended strand and loop regions (Figs. 1B and 2). Two four-helix bundles (α -helices B, C, E, and F and α -helices K, L, N, and O) are the main structural motifs of the tertiary structure and are spatially related by a rotation of about 180° around an axis perpendicular to the sketch plane in Fig. 2. These helices are between 14 and 31 residues long. α -Helices G and S are each packed against one of the four-helix bundles, and α -helices I and J are located on top of the four-helix bundles and approximately perpendicular to their helical axes. There are eight short helices found in connecting segments. Four of them are α -helical (H, M, P, and Q in Figs. 1B and 2), and the other four are 3_{10} -helices (A, D, R, and T in Figs. 1B and 2). At a first glance, the compact α -helical structure of CPO resembles those of the R2 subunit of ribonucleotide reductase from *Escherichia coli* (28) and the first domain of the α subunit and the β subunit of the hydroxylase protein of methane monooxygenase from *Methylococcus capsulatus* (Bath) (29), both nonheme di-iron proteins. However, the main motif in both nonheme di-iron proteins is an eight-helix bundle with a special topological sequence and arrangement of the α -helices different from that found here. Recently, the crystal structure of a bacterial bromoperoxidase (30) has been determined. This enzyme lacks cofactors and shows the general topology of the α/β hydrolase fold. Apparently, the vanadium CPO and the bacterial bromoperoxidase lack any structural similarities and are very different enzymes.

Vanadium Binding Site. The vanadium center is located on top of the second four-helix bundle (Fig. 1A), and the residues forming the metal binding site are coming from helices J, L, N, and O and from turns 290–294, 355–363, 395–406, and 492–502 (Fig. 3). Thus, all residues building up the metal center are from the C-terminal half of the molecule. In our structure with a 2 mM azide mother liquor concentration, the vanadium has a trigonal bipyramidal coordination with three nonprotein

[‡]The atomic coordinates and structure factors have been deposited in the Protein Data Bank, Chemistry Department, Brookhaven National Laboratory, Upton, NY 11973 (identification code 1V NC). This information is embargoed for 9 months (coordinates) and 9 months (structure factors) from the date of publication.

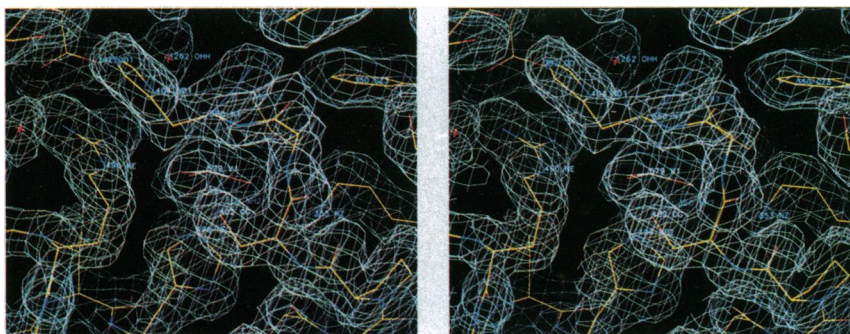


FIG. 4. Final $2|F_o| - |F_c|$ electron density map in the vicinity of the vanadium center at 2.1 \AA resolution [program o (21)]. The map has been contoured at 1.0σ above background.

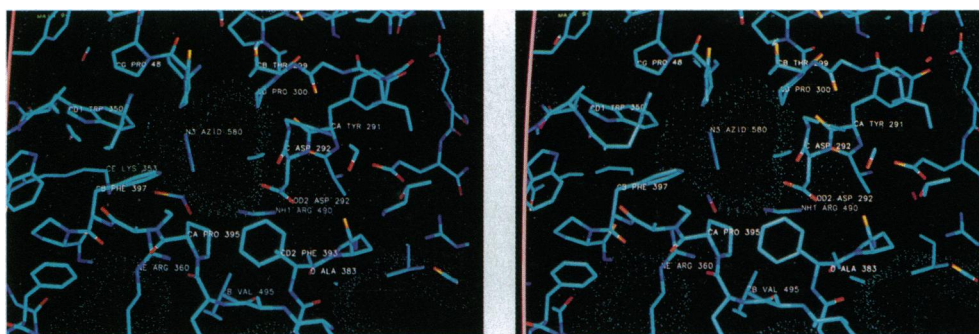


FIG. 5. Stereoview of the channel leading to the vanadium binding site. The solvent molecules in the channel have been omitted. A van der Waals surface is shown. The figure has been made by program MAIN (31).

oxygen ligands (bond distances of about 1.65 Å), one nitrogen ligand (N^{e2} atom) from His-496 (bond distance of 2.25 Å), and an exogenous azide ligand (bond distance to coordinating nitrogen of 1.98 Å). A stereoview of the atomic model and the $2|F_o| - |F_c|$ electron density map around the vanadium center is shown in Fig. 4. It demonstrates the good quality of the electron density map and the clear definition of the azide group.

The negative charge of the VO₃ group with vanadium in the oxidation state (V) is compensated by hydrogen bonds to several positively charged protein side chains and the main chain amide nitrogen of Gly-403 (Fig. 3). Oxygen O^{ω1} of the VO₃ group makes hydrogen bonds to nitrogens N^{η1} of Arg-360 (2.94 Å) and N^{η2} of Arg-490 (2.93 Å), oxygen O^{ω2} to nitrogen N^ξ of Lys-353 (2.72 Å) and nitrogen N of Gly-403 (2.99 Å), and oxygen O^{ω3} to oxygen O^γ of Ser-402 (2.71 Å) and nitrogen N^ε of Arg-490 (3.04 Å). A water molecule from solvent is hydrogen bonded to the nitrogen atom N1 of the bound azide molecule. Preliminary azide inhibition studies on CPO from *C. inaequalis* reveal that inhibition occurs at already very low concentrations (<1 μM) (P. Barnett and R.W., unpublished results).

The binding of the vanadium as hydrogen vanadate(V) has now been confirmed by a difference Fourier map of the azide-free form, which was calculated as described before. This difference map contains as highest peaks the VO₄ group and one water molecule hydrogen bonded to the apical oxygen atom. The difference density has the shape of a trigonal pyramid with the vanadium in the center of the trigonal base plane, three oxygens at the vertices of this plane, and the fourth oxygen at the apex of the pyramid. The N^{e2} atom from His-496 completes the trigonal bipyramidal coordination of the vanadium. Exact bond lengths and angles of the vanadium binding site of the azide-free form will be available after crystallographic refinement of the azide-free form. As Fig. 4 shows, the

CPO	343	TDAGIFSWKEKWEF-EFWRPLS-GV
BRPO	14	ELAQRSSWYQNWQVHRFARPEALGG
Consensus		A SW W F RP G
Function		◇ ◇
CPO	393	FKPPFPAYPSGHATFGGAVFQMVERRY
BRPO	90	GTPTHPSPYPSGHATXNGAFATVLKAL
Consensus		P P YPSGHAT GA
Function		◇◇●
CPO	480	WELMFENAIISRIFLGVHWRFDAAA
BRPO	152	KKLAVNVAFGRQMLGIHYRFDGIQ
Consensus		L A R LG H RFD
Function		◇ *

FIG. 6. Amino acid sequence alignment of stretches of high similarities of CPO (6) and vanadium-containing bromoperoxidase from *A. nodosum* (BRPO) (38). The alignment was carried out manually. *, Protein ligand directly bound to vanadium; ◇, residue hydrogen bonded to vanadate oxygen; ●, catalytic histidine.

binding site for the hydrogen vanadate(V) is a pocket preformed by the protein, which is located at the end of a broad channel (Fig. 5) filled by solvent molecules (omitted in the figure). This channel supplies good access and release for the substrates and products of the enzymatic reaction. One contiguous half of its surface is mainly hydrophobic with Pro-47, Pro-211, Trp-350, Phe-393, Pro-395, Pro-396, and Phe-397 as contributing side chains. The other half is predominantly polar with several main chain carbonyl oxygens and the ion pair Arg-490–Asp-292. It is intriguing that the vanadium(V) is bound directly as hydrogen vanadate(V) with one immediate protein ligand only.

Mechanistic Aspects. Steady-state kinetic studies on CPO (5) show that in the pH range between 6 and 7 the enzyme mechanism is a ping-pong type. The available structural data allow us to speculate about the catalytic mechanism on an atomic basis. It is very likely that the azide binding site is the binding site for the peroxide as well. It is directly accessible from the solvent channel, and azide is an inhibitor for CPO. The peroxide will probably be bound in an η² side-on fashion as in many other vanadium peroxide complexes (7, 32). However an end-on binding mode as HO₂⁻ is also conceivable. The next step in the mechanism would then be the binding of the chloride ion to the activated peroxide. Three residues near the azide or peroxide binding site deserve special interest, the hydrophobic side chains of Trp-350 and Phe-397 as well as the imidazole ring of His-404 (Fig. 3). Both hydrophobic side chains provide a hydrophobic environment, which seems to be necessary to stabilize the chloride binding. This has been found in chloride binding sites of various amylases where one side chain close to the chloride ion is donated from a hydrophobic residue (33). Similarly, in the haloalkane dehalogenase of *Xanthobacter autotrophicus* two tryptophan residues are present involved in halogen and halide binding (34).

His-404 is on the other side of the chloride binding site and may play a crucial role as an acid-base group in catalysis. Steady-state kinetic data of the vanadium chloroperoxidase show (5) that binding of hydrogen peroxide is inhibited when a group with a pK_a larger than 5 is protonated. It may be that when His-404 is protonated binding of peroxide to the metal site is no longer possible as is also seen in heme iron peroxidases. This suggests some analogy to the reaction of heme-containing cytochrome *c* peroxidase (35) with peroxide and the vanadium enzyme.

Without proper knowledge of the true nature of the peroxide or peroxo intermediate formed, it is difficult to predict the exact sequence of events occurring after the formation of the peroxo intermediate. Steady-state studies show that the K_m for Cl⁻ is dependent on pH, suggesting that the chloride binds only when a proton has been taken up by the activated peroxo complex. A nucleophilic attack of the chloride on the activated peroxide is probably the next step. This is similar to that proposed for the reaction between Br⁻ and the adduct of hydrogen peroxide and methylrhodium trioxide (13), although

the possibility cannot be excluded that halide oxidation occurs by coordination to the metal (12). Whatever the exact mechanism, a short-lived HOCl intermediate is formed by the enzyme, and it is likely that His-404 acts as proton donor.

Thermostability. CPO exhibits a high thermostability and a high stability in organic solvents (5). The structural and genetic analysis of protein stability by Matthews and associates (36) demonstrated the main factors in stabilizing globular proteins. The effect of disulfide bridges need not to be considered here since they are absent in CPO. The major factor is the hydrophobic effect followed by a minor contribution of electrostatic interactions. The intramolecular ion pairs of CPO were analyzed to assess the electrostatic effect on stabilizing the CPO structure. CPO contains 42 intramolecular ion pairs, four of them with a surface accessibility area of 0.0 Å². In comparison, ascorbate oxidase, a copper protein of similar size (552 residues) and not thermostable, has 42 intramolecular ion pairs in which eight of them exhibit a surface accessibility area of 0.0 Å² (37). Thus, the electrostatic contribution is not responsible for the high stability of CPO, and we conclude that the high stability is mainly due to the compact packing of helices, which reveals a strong stabilizing hydrophobic effect.

Sequence Comparison with Vanadium-Containing Bromoperoxidase from *Ascophyllum nodosum*. An amino acid sequence alignment of the sequence of CPO with the recently determined partial sequence (236 residues) of the vanadium-containing bromoperoxidase from *A. nodosum* (38) has been carried out, and the regions of high similarities are shown in Fig. 6. There are three stretches of high similarity in the regions of residues providing the vanadium histidine ligand (His-496), the vanadate-interacting residues (Arg-360, Ser-402, Gly-403, Arg-490), and the catalytic His-404. Lys-353 has been mutated to an asparagine, which can form a hydrogen bond to O^{ω2} as well. The alignment demonstrates that the metal binding sites in both vanadium-containing haloperoxidases and the overall protein fold will be very similar, reflecting the close relationship of both enzymes.

We thank Professor R. Huber for supporting this project and for valuable suggestions, Dr. J. W. P. M. van Schijndel for supplying the purified CPO, and Ms. E. G. M. Vollenbroek for her help in culturing fungi. A.M. thanks the Deutsche Forschungsgemeinschaft (Schwerpunktthema: Bioanorganische Chemie) for financial support. This work was also supported by grants from the Netherlands Foundation for Chemical Research (SON) and was made possible by financial support from the Netherlands Organization for Scientific Research (NWO) and the Netherlands Technology Foundation (STW).

- Vilter, H. (1984) *Phytochemistry* **23**, 1387–1390.
- de Boer, E., van Kooyk, Y., Tromp, M. G. M., Plat, H. & Wever, R. (1986) *Biochim. Biophys. Acta* **869**, 48–53.
- Wever, R., Tromp, M. G. M., Krenn, B. E., Maryani, A. & van Tol, M. (1991) *Environ. Sci. Technol.* **25**, 446–449.
- van Schijndel, J. W. P. M., Vollenbroek, E. G. M. & Wever, R. (1993) *Biochim. Biophys. Acta* **1161**, 249–256.
- van Schijndel, J. W. P. M., Barnett, P., Roelse, J., Vollenbroek, E. G. M. & Wever, R. (1994) *Eur. J. Biochem.* **225**, 151–157.
- Simons, B. H., Barnett, P., Vollenbroek, E. G. M., Dekker, H. L., Muijers, A. O. & Wever, R. (1995) *Eur. J. Biochem.* **229**, 566–574.
- Wever, R. & Kustin, K. (1990) *Adv. Inorg. Chem.* **35**, 81–115.
- Arber, J. M., de Boer, E., Garner, C. D., Hasnain, S. S. & Wever, R. (1989) *Biochemistry* **28**, 7678–7973.
- Carrano, C. J., Mohan, M., Holmes, S. M., de la Rosa, R., Butler, A., Charnock, J. M. & Garner, C. D. (1994) *Inorg. Chem.* **33**, 646–653.
- de Boer, E., Keijzers, C. P., Klaassen, A. A. K., Reijerse, E. J., Collison, D., Garner, C. D. & Wever, R. (1988) *FEBS Lett.* **235**, 93–97.
- de Boer, E., Boon, K. & Wever, R. (1988) *Biochemistry* **27**, 1629–1635.
- Meister, G. E. & Butler, A. (1994) *Inorg. Chem.* **33**, 3269–3279.
- Espenson, J. H., Pestovsky, O., Huston, P. & Staudt, S. (1994) *J. Am. Chem. Soc.* **116**, 2869–2877.
- Vilter, H. (1989) *Proc. Int. Conf. Coord. Chem. 17th*, M62 (abstr.).
- van Schijndel, J. W. P. M., Simon, L. H., Vollenbroek, E. G. M. & Wever, R. (1993) *FEBS Lett.* **336**, 239–242.
- Leslie, A. G. W. (1990) in *Crystallographic Computing*, eds Moras, D., Podjarny, A. D. & Thierry, J. C. (Oxford Univ. Press, Oxford), Vol. 5, pp. 50–61.
- CCP4 (1990) *Acta Crystallogr.* **D50**, 760–763.
- Steigemann, W. (1974) Ph.D. thesis (Univ. of Munich, Munich, Germany).
- Otwinski, Z. (1991) *MLPHARE, CCP4 Proc* 80–88 (Daresbury Lab., Warrington, U.K.).
- Jones, T. A. & Thirup, S. (1985) *EMBO J.* **5**, 819–822.
- Jones, T. A., You, J. Y., Cowan, S. W. & Kjeldgaard, M. (1991) *Acta Crystallogr.* **A47**, 110–119.
- Brünger, A. T. (1992) xPLOR, Version 3.1: A System for Crystallography and NMR (Yale Univ. Press, New Haven, CT).
- Engh, R. A. & Huber, R. (1991) *Acta Crystallogr.* **A47**, 392–400.
- Aschwendt, S., Schmalle, H. W., Reller, A. & Oswald, H. R. (1993) *Mater. Res. Bull.* **28**, 575–579.
- Hanich, J., Krestel, M., Müller, U., Dehnicke, K. & Rehder, D. (1984) *Z. Naturforsch. B Chem. Sci.* **39**, 1686–1695.
- Kraulis, P. (1991) *J. Appl. Crystallogr.* **24**, 946–950.
- Kabsch, W. & Sander, C. (1983) *Biopolymers* **22**, 2577–2637.
- Nordlund, P., Sjöberg, B.-M. & Eklund, H. (1990) *Nature (London)* **345**, 593–598.
- Rosenzweig, A. C., Frederick, C. A., Lippard, S. J. & Nordlund, P. (1993) *Nature (London)* **366**, 537–543.
- Hecht, H. J., Sonek, H., Haag, T., Pfeifer, O. & van Pée, K.-H. (1994) *Nat. Struct. Biol.* **1**, 532–537.
- Turk, D. (1994) Ph.D. thesis (Univ. of Munich, Munich, Germany).
- Butler, A., Calgus, M. J. & Meister, G. E. (1994) *Chem. Rev.* **94**, 625–638.
- Machius, M., Wiegand, G. & Huber, R. (1995) *J. Mol. Biol.* **246**, 545–559.
- Verschuere, K. H. G., Kingma, J., Rozeboom, H. J., Kalk, K. H., Janssen, D. B. & Dijkstra, B. W. (1993) *Biochemistry* **32**, 9031–9037.
- Poulos, T. L. & Kraut, J. (1980) *J. Biol. Chem.* **255**, 8199–8205.
- Matthews, B. W. (1993) *Annu. Rev. Biochem.* **62**, 139–160.
- Messerschmidt, A., Ladenstein, R., Huber, R., Bolognesi, M., Avigliano, L., Petruzzelli, R. & Finazzi-Agró, A. (1992) *J. Mol. Biol.* **224**, 179–205.
- Vilter, H. (1995) in *Metal Ions in Biological Systems*, eds Sigel, H. & Sigel, A. (Dekker, New York), Vol. 31, pp. 326–362.